

## Article

# The Synthesis and Reactivity of Mesoporous and Surface-Rough Vinyl-Containing ORMOSIL Nanoparticles

Nathan I. Walton, Eric M. Brozek, Courtney C. Gwinn and Ilya Zharov \* 

Department of Chemistry, University of Utah, 315 South 1400 East, Salt Lake City, UT 84112, USA; nathanwalton34@gmail.com (N.I.W.); e.m.brozek@gmail.com (E.M.B.); c.gwinn@advancederm-hub.com (C.C.G.)  
\* Correspondence: i.zharov@utah.edu

**Abstract:** Silica nanoparticles synthesized solely from organosilanes naturally possess a greater number of organic functionalities than silica nanoparticles surface-modified with organosilanes. We report the synthesis of organically modified silica (ORMOSIL) nanoparticles with a mesoporous and surface-rough morphology and with a high surface area, made solely from vinyltrimethoxy silane. We chemically modified these vinyl silica nanoparticles using bromination and hydroboration, and demonstrated the high accessibility and reactivity of the vinyl groups with an ~85% conversion of the functional groups for the bromination of both particle types, a ~60% conversion of the functional groups for the hydroboration of surface-rough particles and a 90% conversion of the functional groups for the hydroboration of mesoporous particles. We determined that the mesoporous vinyl silica nanoparticles, while having a surface area that lies between the non-porous and surface-rough vinyl silica nanoparticles, provide the greatest accessibility to the vinyl groups for boronation and allow for the incorporating of up to  $3.1 \times 10^6$  B atoms per particle, making the resulting materials attractive for boron neutron capture therapy.

**Keywords:** organosilica; nanoparticle; mesoporous; vinyl; hydroboration; bromination



**Citation:** Walton, N.I.; Brozek, E.M.; Gwinn, C.C.; Zharov, I. The Synthesis and Reactivity of Mesoporous and Surface-Rough Vinyl-Containing ORMOSIL Nanoparticles. *Colloids Interfaces* **2024**, *8*, 18. <https://doi.org/10.3390/colloids8020018>

Academic Editor: Reinhard Miller

Received: 29 November 2023

Revised: 29 February 2024

Accepted: 4 March 2024

Published: 7 March 2024



**Copyright:** © 2024 by the authors. Licensee MDPI, Basel, Switzerland. This article is an open access article distributed under the terms and conditions of the Creative Commons Attribution (CC BY) license (<https://creativecommons.org/licenses/by/4.0/>).

## 1. Introduction

The chemical and thermal robustness, combined with the hydrophilicity of silica nanoparticles, render them effective carriers for diverse organic and inorganic substances [1]. They hold significant promise for uses in optical, imaging, and therapeutic applications [2]. Mesoporous organosilica nanoparticles represent an even more interesting but much less studied class of materials [3,4]. While silica inherently have only the silanol reactive groups, the introduction of organosilanes gives them beneficial organic features [5]. They combine the properties of organic and silica materials and have emerged as a class of hybrid materials with diverse potential applications in catalysis, drug delivery, imaging, and more. Organosilanes can alter the surface charge and polarity of these nanoparticles, and offer options for further modifications using conventional synthesis methods [6].

Silica nanoparticles with mesopores in the range of 2–30 nm are commonly prepared via the condensation of silica precursors (silica alkoxides TEOS, TMOS [7–9], their functionalized derivatives [10], sodium silicates [11]) in the presence of surfactant micelles and a catalyst in an aqueous medium [12]. This process is affected by the surfactant concentration [13,14], the type and amount of the hydrolyzing agents [7,8,15–23], the presence of various kosmotropic and chaotropic salts [12,24–35], alcohol additives [8,9,36–39] and the degree of dilution [8,17,22,40].

Two techniques exist to incorporate organic functional groups within silica: “grafting to” and co-condensation [41]. In the “grafting to” method, silica nanoparticles are modified after creation through a reaction that uses an organosilane, causing a hydrolysis/condensation process. This not only maintains the nanoparticle’s initial shape but also adds organic functions to its surface. Several organic groups can be incorporated due to the

ability of organosilanes to partake in the condensation. For example, the surfaces of silica nanoparticles were modified with methyl, vinyl, amino, and mercapto trialkoxy silanes using a two-step sol–gel process. In the first step, TEOS was hydrolyzed and condensed to form silica nanoparticles. Second, the hydrolysis and condensation of the organosilane was performed in the presence of the newly formed silica nanoparticles. The organosilanes reacted with the silanol groups on the surfaces of the silica particles causing the surface modification [42]. The addition of organosilanes to the surfaces of silica particles is relatively simple in terms of synthesis; however, the distribution of organosilanes on the particle surface is difficult to control [43]. For porous particles, the pore openings may also become blocked by the added organosilanes.

The co-condensation technique offers organically modified silica (ORMOSIL) nanoparticles infused with organic functionalities distributed throughout their structure [2,44]. In most cases, the co-condensation involves the use of TEOS as the main source of silica together with organosilane precursors in the presence of a base catalyst in water/ethanol solvent mixtures. Typically, organosilane precursors possess three ethoxy or methoxy groups and one organic group such as methyl, ethyl, vinyl, phenyl, pentyl, octyl, phenyl and aminopropyl [45,46]. The silicon–carbon bonds remain stable during the hydrolysis–condensation process and the resulting particles possess low surface areas ( $<100 \text{ m}^2 \text{ g}^{-1}$ ) with 2–4 nm mesopores arising from the steric effects of the organic groups. The use of organosilanes as the sole precursors for organosilane nanoparticles is less common due to the difficulties controlling the resulting morphologies [47,48].

While the co-condensation leads to a larger count of organic groups, they can be hard to modify later, typically necessitating prior selection (e.g., the covalent encapsulation of a fluorophore) [49,50]. Mostly, only those organic functional groups on the silica exterior are accessible and apparently abundant in both methods. Increasing the ratio of the silica nanoparticles' surface area to volume would enhance the organic functions' accessibility. This involves the creation of particles with rough surfaces or mesoporous structures [51,52]. Despite both types of particles possessing extensive surface areas, their utility differs vastly. Rough surface silica nanoparticles are prepared either by etching the silica particles [53] or incorporating smaller spheres onto bigger ones [51]. When merged with water-repelling organosilanes, these nanoparticles adopt very hydrophobic traits, proving useful in the production of water-repellent glass [54,55].

On the other hand, mesoporous particles are produced in the presence of surfactant micelles that direct the mesoporous silica formation [56]. Cetyltrimethylammonium bromide (CTAB) is a typical surfactant in these processes, which leads to a higher surface area and silanol group availability, paving the way for added modifications. In these nanoparticles, the mesoporous structure grants more organic group access via the pores. Consequently, these particles have been applied in drug delivery [57,58] and imaging [59–61] due to their ability to encapsulate therapeutic and/or imaging agents.

Increasing the number of organic functional groups can enhance the usefulness of silica nanoparticles. Thus, preparing such particles solely from functional organosilanes would be advantageous. In such particles, the organic functions become more accessible as the silica framework becomes altered due to replacing the Si–O bonds with bonds to organic groups, and due to steric factors, leading to some porosity [62]. Like traditional particles, enhancing these nanoparticles' surface area by adding mesopores can amplify the organic functions' accessibility even further. Yet, preparing these nanoparticles remains a challenge [63,64].

ORMOSIL nanoparticles containing vinyl groups are of interest because these functional groups can undergo further transformations using well-established alkene reactions, such as to bromination, hydroxylation and hydroboration [62]. The result of the latter are nanoparticles containing large amounts of boron, which constitute attractive agents for the boron neutron capture therapy (BNCT) of cancer, the process where  $^{10}\text{B}$  nuclei undergo a localized fission reaction and emit alpha particles capable of destroying cancer cells [65].

Our research on the preparation of organosilica nanoparticles initially focused on the synthesis of the particles incorporating reactive functional groups using the co-condensation of organosilanes with tetraethoxysilane. For example, we prepared [62] non-porous vinyl-silsesquioxane nanoparticles and showed that the vinyl groups inside the nanoparticles can be easily brominated or hydroborated, leading to the nanoparticles containing 59.9 wt% of bromine or 3.6 wt% of boron, respectively. We also designed, prepared, and characterized [66] hydrolysable organosilica nanoparticles (ICPTES-Sorbitol SNPs) via the co-condensation of tetraethoxysilane with a bridged sorbitol-based silsesquioxane precursor containing carbamate linkages. We later shifted our focus to a novel method for the preparation of mesoporous particles [67] and to the preparation of organosilica nanoparticles using organosilanes as the sole precursors [68]. We also prepared [69,70] organosilica nanoparticles with internal metal-chelating diethylenetriametetraacetic acid groups (DTTA-MSNPs) via co-condensation and studied the binding of transition metal ions such as copper (II), cobalt (II) and gadolinium (III) by DTTA-MSNPs.

Given the importance of ORMOSIL nanoparticles, particularly those with mesopores and with reactive organic functional groups, and the limited synthetic approaches available for their preparation, we decided to explore the preparation of such particles further. Our current paper describes the results of our efforts, namely two synthetic methods for the preparation of novel large surface area vinyl ORMOSIL nanoparticles using the corresponding organosilane as a sole precursor. These methods use micellar solutions to create mesoporous and surface-rough nanoparticles. The paper also describes the organic transformations of the vinyl groups inside the porous and surface-rough ORMOSIL nanoparticles, and the results are compared to determine the extent of the vinyl group transformation.

## 2. Materials and Methods

**Materials.** The following materials were used as received: vinyltrimethoxy silane (VTMS, 97%, Gelest Inc., Morrisville, PA, USA), hexadecyltrimethylammonium bromide (CTAB, 99.0%, Sigma-Aldrich, St. Louis, MO, USA), mesitylene (1,3,5-trimethylbenzene, TMB, 97%, Sigma-Aldrich), ethylene glycol (EG, 99%, VWR Inc, West Chester, PA, USA), ammonium hydroxide (28–30%, Sigma-Aldrich), 1 M of borane in tetrahydrofuran (Sigma-Aldrich), bromine (Sigma-Aldrich), hydrochloric acid (concentrated, Fluka) and ethanol (anhydrous, Decon Labs Inc., King of Prussia, PA, USA).

**Instruments.** Transmission electron microscopy was performed using an FEI Techna G2 T-12 microscope with an acceleration voltage of 120 kV. Average particle size and standard deviation were calculated from measuring 150–250 particles using the ImageJ software Version 1.53s (19 May 2022). FT-IR spectroscopy was performed using Bruker Tensor 37. Nitrogen adsorption–desorption analysis was performed using Micrometrics ASAP 2020. The degassing procedure was carried out at 200 °C for 4 h under a 1 µm Hg vacuum, and the isotherm was recorded in the pressure range of  $P/P_0 = 0.002 - 0.99$ . The specific surface areas were calculated using the multipoint BET method at  $P/P_0 = 0.05 - 0.25$ , the pore size distributions—by the BJH (cylindrical pores) on the adsorption branch of the isotherm. The thermogravimetric analysis was performed using a TA Instruments 2950 Thermogravimetric Analyzer for vacuum-dried particles at a heating rate of 10 °C/min from room temperature to 800 °C under the N<sub>2</sub> atmosphere. The percent of the vinyl groups was calculated using the following equation:

$$\frac{\rho \cdot \frac{4}{3} \cdot \pi \cdot r_{(\text{cm})}^3 \cdot \%W_{\text{lossVNP}}}{100 \cdot MW_{\text{vinyl}}} = \frac{\text{mol vinyl}}{\text{particle}} \quad (1)$$

where  $\rho$  is the particle density in  $\text{g} \cdot \text{cm}^{-3}$  (~1.35),  $r$  is the particle radius,  $MW_{\text{vinyl}}$  is the molecular weight of the vinyl group, and  $\%W_{\text{loss}}$  is the TGA-measured weight loss of

the vSNPs. The percent conversion of the vinyl groups was calculated using the following equation:

$$\frac{\rho \cdot \frac{4}{3} \cdot \pi \cdot r(\text{cm})^3 \cdot (\%W_{\text{lossVNP+X}} - \%W_{\text{lossVNP}})}{100 \cdot MW_X} = \frac{\text{mol X}}{\text{particle}} \quad (2)$$

where  $\rho$  is the particle density in  $\text{g} \cdot \text{cm}^{-3}$  ( $\sim 1.35$ ),  $r$  is the particle radius,  $MW_X$  is the molecular weight of the vinyl group, and  $\%W_{\text{loss}}$  is the TGA-measured weight loss of the nanoparticles. The percentage of vinyl groups that reacted in bromination or hydroboration was calculated using the following equation:

$$\frac{\text{mol X}}{\text{particle}} \div \frac{\text{mol vinyl}}{\text{particle}} \times 100 = \text{mol \% conversion} \quad (3)$$

**Mesoporous vinyl silica nanoparticle synthesis.** CTAB (0.587 g, 1.61 mmol), ethanol (43 mL), EG (15 mL) and 28%  $\text{NH}_4\text{OH}$  (3.6 mL) were dissolved in 90 mL of MilliQ water (MilliporeSigma, Burlington, MA, USA) in a 250 mL round-bottom flask. The solution was stirred rapidly at 70 °C for 25 min. VTMS (0.69 mL, 3.2 mmol) was added to the solution which was stirred for 72 h at room temperature. The resulting particles were collected by centrifugation and washed 3 times with 10 mL of ethanol. The particles were then added to 30 mL of the ethanolic solution of 1 M of HCl in a 100 mL round-bottom flask and heated at 80 °C for 12 h to remove the CTAB. The particles were collected and washed 3 times with 10 mL of ethanol.

**Surface-rough vinyl silica nanoparticle synthesis.** CTAB (0.587 g, 1.61 mmol), TMB (0.66 mL, 4.74 mmol, 2.95:1 TMB:CTAB), EG (15 mL), ethanol (43 mL) and 28%  $\text{NH}_4\text{OH}$  (3.6 mL) were dissolved in 90 mL of MilliQ water in a 250 mL round-bottom flask and were stirred rapidly at 70 °C for 25 min. VTMS (0.69 mL, 3.2 mmol) was then added to the solution which was stirred for 72 h at room temperature. The resulting particles were collected by centrifugation and washed 3 times with 10 mL of ethanol. The particles were then added to 30 mL of the ethanolic solution of 1 M of HCl in a 100 mL round-bottom flask and heated at 80 °C for 12 h to remove the CTAB. The particles were collected and washed 3 times with 10 mL of ethanol.

**Bromination of vinyl silica particles.** Vinyl silica nanoparticles (0.1 g, 1.25 mmol) were placed in a scintillation vial containing 10 mL of dichloromethane and sonicated until the particles were well dispersed. Bromine (0.19 mL, 3.75 mmol) was added to the solution followed by a brief sonication. The reaction mixture was stirred overnight at room temperature. The particles were collected via centrifugation and washed five times with 10 mL of dichloromethane to completely remove the bromine.

**Hydroboration of vinyl silica particles.** Under the nitrogen atmosphere, vinyl silica nanoparticles (0.1 g) were placed in 5 mL of 1 M  $\text{BH}_3 \cdot \text{THF}$  (5 mL) in a 25 mL round-bottom flask and 6 mL of THF were added. The reaction mixture was stirred for 3 h, sonicated and then stirred again overnight at room temperature. The particles were then collected and washed three times with 10 mL of THF to remove excess  $\text{BH}_3 \cdot \text{THF}$ , followed by washing with a 9:1 ethanol-water mixture and sonication in 10 mL of MilliQ water to complete the conversion to boric acids. Finally, the particles were washed twice with 10 mL of MilliQ water.

### 3. Results and Discussion

Synthesis of vinyl containing ORMOSIL nanoparticles. There are a limited number of organosilane precursors currently known to produce ORMOSIL nanoparticles [71]. Among them, the vinyltrimethoxy silane (VTMS) is noteworthy, especially given its ability to hydrolyze and condense under Stöber conditions [72]. Previously, we reported the formation, characterization and reactivity of ORMOSIL nanoparticles prepared using VTMS [62,68].

By introducing cetyltrimethylammonium bromide (CTAB) and ethylene glycol to VTMS, we successfully prepared mesoporous vinyl silica nanoparticles (mVSNP, Table 1).

CTAB is responsible for micelle formation which then results in mesopore creation, while ethylene glycol augments solution viscosity. This aids in silica nuclei production, controlling particle dimensions and ensuring consistency. The concentrations of ethylene glycol, water, and ethanol greatly influence mVSNP generation [73].

**Table 1.** Characteristics of the synthesized nanoparticles.

Particles	Size, nm	Surface Area, $\text{m}^2 \cdot \text{g}^{-1}$	Calculated Pore Size, nm
mVSNPs	$137 \pm 8$	44.0	37–50
rVSNPs	$97 \pm 6$	278.7	18 *
sVSNPs	$592 \pm 18$	8.5	0

\* Due to surface roughness rather than “through-and-through” pores.

We identified certain conditions hindering mVSNP formation. Without an optimal ethanol/water ratio or an insufficient reaction duration (less than 72 h), the particles either are not formed, or a gel is produced. The gel is also produced if ethanol is added after VTMS. At a reaction temperature below  $50^\circ\text{C}$ , the resulting porosity was also significantly reduced.

Transmission electron microscopy (TEM) revealed porous spherical mVSNPs with an average particle diameter of  $137 \pm 8$  nm and with pores of varied sizes randomly distributed throughout the ORMOSIL particle structure (Figure 1A,B). The fluctuating pore dimensions might be attributed to the VTMS precursor interacting with the hydrophobic core of the micelles, potentially explaining the lower yield, especially if pore interconnection happens during synthesis.

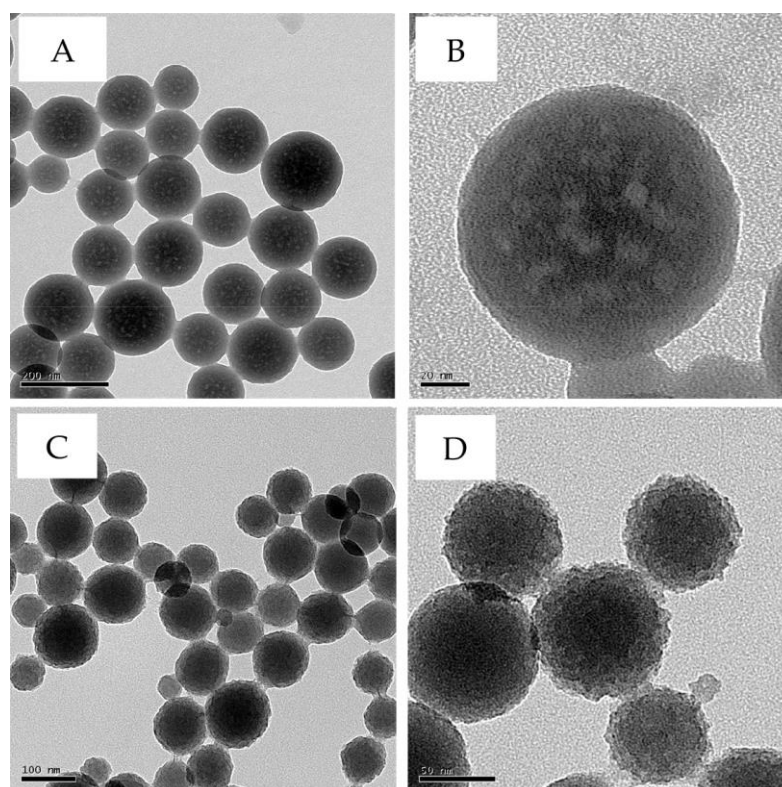


**Figure 1.** TEM images of mVSNPs (A,B) and rVSNPs (C,D). Scale bars are 200 nm (A), 20 nm (B), 100 nm (C) and 50 nm (D).

The disordered pore morphology of mVSNPs is significantly different from that of ordered MSNPs prepared using TEOS as the sole precursor in the presence of CTAB surfactant. However, this is not surprising given that the pore morphology in silica nanoparticles is governed by electrostatic interactions between  $\equiv\text{Si}-\text{O}^-$  and  $\text{CTA}^+$  [12]. These interactions

are expected to be affected by the presence of the organic groups present in the silica precursor used. The type of the particle mesoporosity will also reflect the contribution of cooperative silica-surfactant self-assembly to the particle formation mechanism [12]. Therefore, it is not surprising that mVSNPs' pore morphology resembles that of dendritic mesoporous organosilica nanoparticles [74].

An example of the mVSNPs' nitrogen sorption isotherm is shown in Figure 2A. This isotherm has an expected large nitrogen absorption ( $\sim 260 \text{ cm}^3 \cdot \text{g}^{-1}$  STP) and appears to be type II. However, it has an H1 hysteresis loop between 0.92 to 1  $P/P_0$ , indicating mesoporosity, and therefore, it is probably a type IV without the noticeable plateau, which is not uncommon for mesoporous materials [51,75]. Using this isotherm, we calculated the pore diameters for the mVSNPs and found a wide distribution of sizes from 2 nm to 50 nm (Figure 2B). The pore size distribution showed the periodic pore size maxima from 2 nm to  $\sim 30$  nm (2, 7, 12, 18, and 23 nm) demonstrating that the mesopores are not uniform in size. We used a BJH model to calculate the average pore sizes of the mVSNPs. It should be noted that the BJH model is based on a model of cylindrical pores [76] while mVSNPs contain pores of an irregular morphology. However, this model is commonly applied to dendritic mesoporous nanoparticles which possess a similar morphology [77], and in the absence of a better model we used a BJH that provided the pore size to be between 37 and 50 nm. This pore size agrees with the pore sizes observed by TEM. A BET analysis of the mVSNP samples gave the surface area of the mVSNP to be in the range of  $30.3\text{--}44.0 \text{ m}^2 \cdot \text{g}^{-1}$ . This surface area is 3.5–5 times larger than that of non-porous sVSNPs, which are discussed below. However, this surface area is lower than that for other reported mesoporous silica particles [29]. Given the large size of the pores in the mVSNPs, the overall lower surface area means that these particles possess a lower pore density.

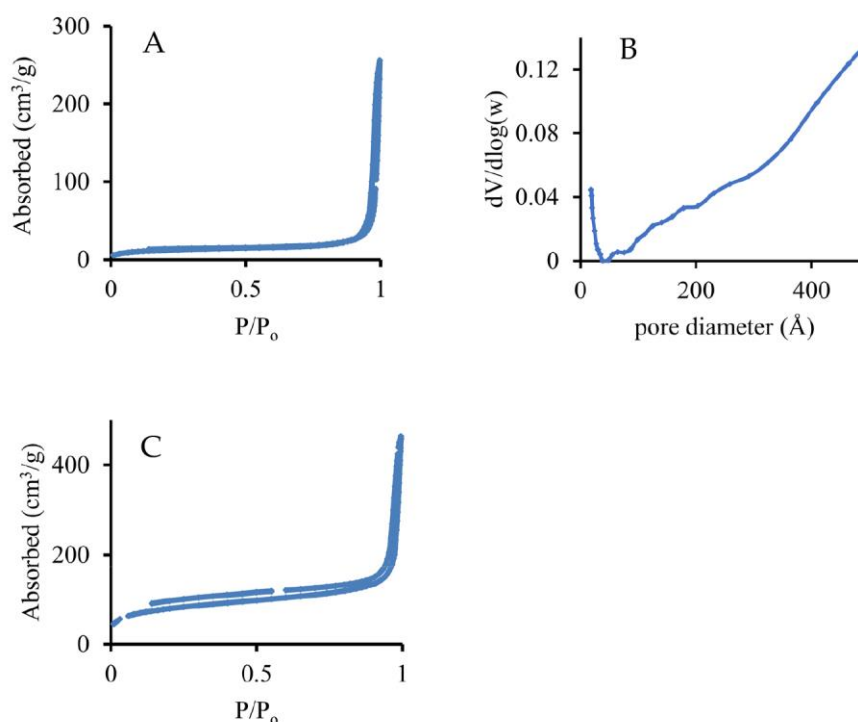


**Figure 2.** Nitrogen adsorption–desorption isotherms of mVSNPs (A) and rVSNPs (C) and the pore size distribution of the mvSNPs (B).

When trimethylbenzene (TMB), a swelling agent, was added before VTMS condensation, we expected the formation of particles with larger pores. Instead, we produced surface-rough particles (rVSNPs, Figure 1C,D, Table 1), possibly because the VTMS could not fully envelop the expanded micelles. However, the yield of these rough-surfaced

particles was higher, perhaps owing to TMB's interaction with VTMS within the micelles. The diameter of these rVSNPs was  $97 \pm 6$  nm and their nitrogen absorption isotherm (Figure 2C) gave a nitrogen adsorption of  $\sim 450 \text{ cm}^3 \cdot \text{g}^{-1}$ , which is higher than that of the mVSNPs. Based on the absence of a "loop" in the hysteresis of the nitrogen sorption isotherm of rVSNPs as opposed to mVSNP, we concluded that rVSNPs contain porous areas with hindered nitrogen exchange. According to the BJH calculations, the size of the pores in rVSNPs is 18.5 nm. This observation is likely due to the cavities created by the rough surface, because if there were "through-and-through" pores of this calculated size, they would be visible by TEM. Finally, the BET surface area of the rVSNPs was determined to be  $278.70 \text{ m}^2 \cdot \text{g}^{-1}$ , significantly larger than that of the mVSNPs. Taken together, our observations from TEM and BET suggest that rVSNPs are mostly non-porous with their morphology and properties defined by their rough surface.

For comparison, non-porous vinyl silica nanoparticles (sVSNPs, Table 1) were also produced without CTAB. These particles were larger, the diameter of sVSNPs of  $592 \pm 18$  nm (Figure 3). The nitrogen adsorption-desorption isotherm analysis of these nanoparticles gave a BET surface area of  $8.5 \text{ m}^2 \cdot \text{g}^{-1}$ . It should also be noted that the sVSNPs absorbed little nitrogen ( $\sim 13 \text{ cm}^3 \cdot \text{g}^{-1}$  STP) and exhibited a type II isotherm (Figure 3), which is indicative of non-porous materials [78].

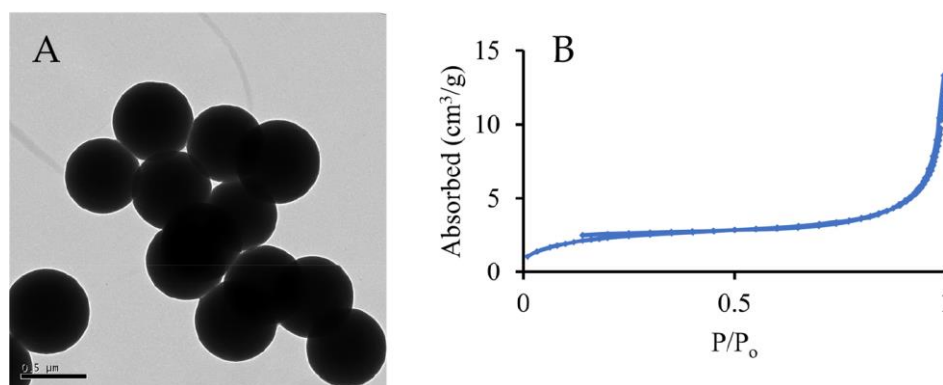
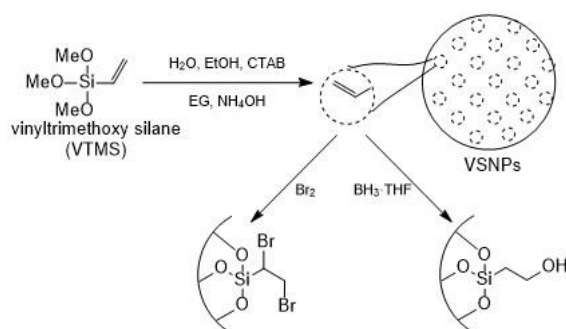


**Figure 3.** (A) TEM image of non-porous sVSNPs formed in the absence of CTAB. Scale bar is 500 nm. (B) A nitrogen adsorption–desorption isotherm of sVSNPs.

Bromination of vinyl silica nanoparticles. Bromination was our chosen model reaction, given the ease with which bromine reacts with alkenes. Upon brominating the vinyl particles (Scheme 1), the characteristic color of bromine vanished, producing a pale powder. To confirm that the bromination indeed took place, we used IR spectroscopy (Figure 4). We observed that the vinyl group stretch at  $960 \text{ cm}^{-1}$  disappeared and the  $1602 \text{ cm}^{-1}$  stretch was greatly reduced. We also observed new bands at  $875$ ,  $760$  and  $650 \text{ cm}^{-1}$ , which correspond to C-Br stretches.



**Scheme 1.** Preparation and chemical modification of vinyl-containing nanoparticles.

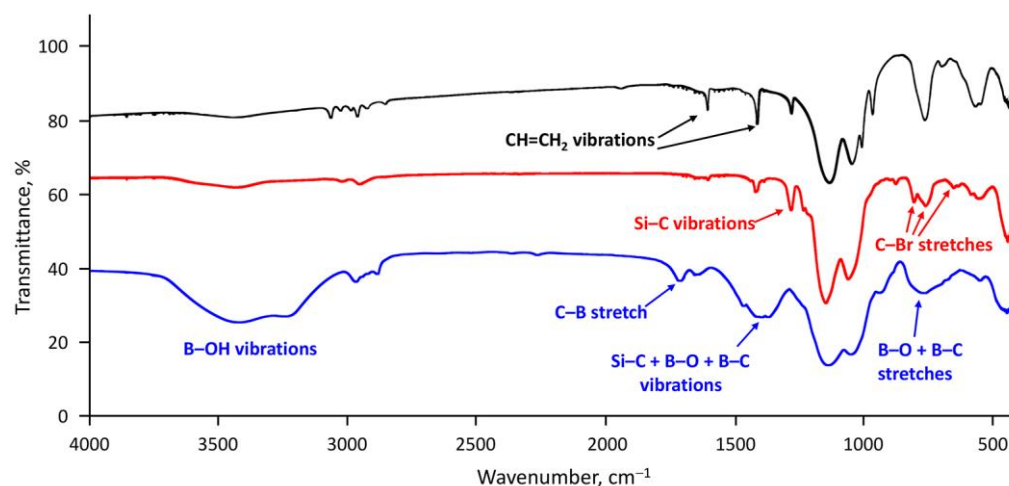


**Figure 4.** IR spectra of unmodified (black), brominated (red), and hydroborated (blue) mVSNPs.

The thermogravimetric analysis (TGA) further confirmed the extensive bromination of the vinyl groups in the prepared nanoparticles. All three types of nanoparticles, sVSNP, rVSNPs and mVSNPs, exhibited a weight loss of ~60% after their bromination (Figure 5). This is significantly higher compared to the weight loss of ~9% observed for these particles before the bromination. Using the TGA weight loss for sVSNP, rVSNPs and mVSNPs, we calculated the percent conversion of the vinyl groups in the bromination reaction to be ~85%. This result suggests that (1) the vinyl groups in all three types of the prepared nanoparticles are accessible and highly reactive, and (2) the accessibility of the vinyl groups to bromine and their reactivity with bromine in all three types of the prepared nanoparticles are similar.

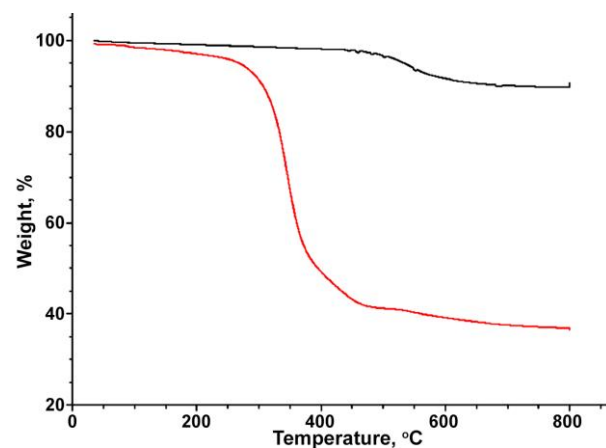


**Figure 5.** TGA weight loss of mVSNPs (black) and brominated mVSNPs (red).

Hydroboration of vinyl silica nanoparticles. To explore potential uses for ORMOSIL particles in boron neutron capture therapy (BNCT), we performed the hydroboration of VSNPs using  $\text{BH}_3 \cdot \text{THF}$ . Infrared spectroscopy (Figure 4) confirmed successful hydroboration, indicating significant chemical changes within the particles. Specifically, the Si-C stretch at  $1410 \text{ cm}^{-1}$  broadened after hydroboration likely due to the appearance of B-O vibrations in the same region. A new band at  $770 \text{ cm}^{-1}$  appeared, corresponding to O-B-O and/or B-C stretches. Another new band, at  $3500 \text{ cm}^{-1}$ , indicated the formation of hydroxyl groups belonging to boric acid. Finally, a new band appeared at  $1712 \text{ cm}^{-1}$ , corresponding to the C-B-C stretch. Based on these observations, we concluded that the vinyl groups inside VSNPs indeed underwent hydroboration and were converted to boric acid. This reaction

also led to a marked difference in particle solubility, with hydroborated particles becoming hydrophilic unlike the starting particles, which were only dispersible in hexane.

Although an elemental analysis can be used to characterize the changes in the elemental composition of these nanoparticles (we used it in our previous work to show the incorporation of boron atoms [62]), TGA provides a more comprehensive picture. A TGA-based comparative study revealed the degree of hydroboration among various VSNP particles. For sVSNPs and rVSNPs, the TGA showed a weight loss of ~9% before the hydroboration. After the hydroboration, the weight loss increased to ~19% for sVSNPs and to ~18% for rVSNPs (Figure 6). Using these results, the conversion of the vinyl groups to boric acid by hydroboration is calculated to be ~58% for sVSNPs and ~56% for rVSNPs. The resulting boron content is  $1.69 \times 10^{21} \text{ B}\cdot\text{cm}^{-3}$  ( $1.8 \times 10^8 \text{ B}$  per particle) for sVSNPs and  $1.56 \times 10^{21} \text{ B}\cdot\text{cm}^{-3}$  ( $7.2 \times 10^5 \text{ B}$  per particle) for rVSNPs. Therefore, sVSNPs and rVSNPs showed very similar behaviors in terms of their hydroboration.

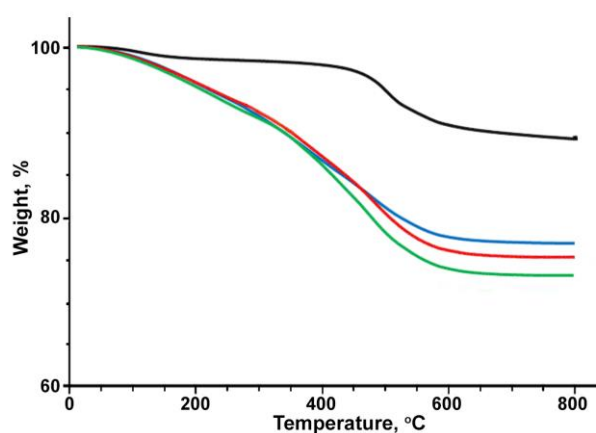


**Figure 6.** TGA weight loss of unmodified sVSNPs (black) and hydroborated sVSNPs (red), rVSNPs (blue), and mVSNPs (green).

In contrast, for mVSNPs, TGA showed a higher weight loss of ~22% (Figure 6), which corresponds to a significantly higher extent of vinyl group conversion to boric acid, at ~90%, or ca. 1.5 times greater than that for sVSNPs or rVSNPs. This also leads to a significantly higher boron loading after the hydroboration of mVSNPs, at  $2.3 \times 10^{21} \text{ B}\cdot\text{cm}^{-3}$  ( $3.1 \times 10^6 \text{ B}$  per particle). We hypothesize that this is the result of the presence of mesopores in mVSNPs that should facilitate the access of the hydroboration agent to the vinyl groups throughout the mVSNP structure. Interestingly, we did not observe such selectivity in the case of bromination, where all three types of prepared nanoparticles showed similar degrees of vinyl group conversion (85%). This is likely due to the much higher reactivity of bromine towards the double bonds, compared to that of  $\text{BH}_3\cdot\text{THF}$ .

The hydroborated mVSNPs are promising theranostic agents [79]. Indeed, they contain over  $10^6$  boron atoms per particle making them suitable for boron neutron capture therapy (BNCT) [65]. They also possess a high surface area and a reactive silica surface suitable for the attachment of imaging moieties and cancer cell-targeting ligands. Overall, organosilica nanoparticles and particularly those containing reactive functional groups find applications in diverse biomedical fields [80–82] as well as in materials [83,84], catalysis [85,86] and environmental remediation [87,88] fields.

#### 4. Conclusions

We developed the synthesis of ORMOSIL nanoparticles with large surface areas and a high content of vinyl functional groups from vinyltrimethoxy silane as a sole precursor. By using a surfactant (CTAB), we created vinyl-containing nanoparticles with mesopores in the 37–50 nm range. When a swelling agent (TMB) was introduced to the reaction mixture, surface-rough vinyl particles (rather than mesoporous particles with larger pores) were

formed. Both particle types possess a high surface area and abundant reactive vinyl groups that can undergo bromination and hydroboration, achieving a high conversion of the vinyl groups. The hydroborated particles can potentially be used as efficient boron carriers for BNCT applications, containing approximately  $10^6$  boron atoms per particle.

**Author Contributions:** Conceptualization, I.Z.; investigation, N.I.W., E.M.B., C.C.G.; data curation, N.I.W.; writing—original draft preparation, N.I.W.; writing—review and editing, I.Z.; supervision, I.Z.; project administration, I.Z.; funding acquisition, I.Z. All authors have read and agreed to the published version of the manuscript.

**Funding:** This research was funded by an Energy Frontier Research Center EFRC-MUSE funded by the US Department of Energy, Office of Science, Basic Energy Sciences, Award #DE-SC0019285.

**Data Availability Statement:** The data presented in this study are available on request from the corresponding author.

**Conflicts of Interest:** The authors declare no conflict of interest.

## References

1. Jeelani, P.G.; Mulay, P.; Venkat, R.; Ramalingam, C. Multifaceted application of silica nanoparticles. A review. *Silicon* **2020**, *12*, 1337–1354. [[CrossRef](#)]
2. Croissant, J.G.; Fatieiev, Y.; Almalik, A.; Khashab, N.M. Mesoporous silica and organosilica nanoparticles: Physical chemistry, biosafety, delivery strategies, and biomedical applications. *Adv. Healthc. Mater.* **2018**, *7*, 1700831. [[CrossRef](#)] [[PubMed](#)]
3. Guan, B.; Cui, Y.; Ren, Z.; Qiao, Z.A.; Wang, L.; Liu, Y.; Huo, Q. Highly ordered periodic mesoporous organosilica nanoparticles with controllable pore structures. *Nanoscale* **2012**, *4*, 6588–6596. [[CrossRef](#)] [[PubMed](#)]
4. Teng, Z.; Li, W.; Tang, Y.; Elzatahry, A.; Lu, G.; Zhao, D. Mesoporous organosilica hollow nanoparticles: Synthesis and applications. *Adv. Mater.* **2019**, *31*, 1707612. [[CrossRef](#)] [[PubMed](#)]
5. Zou, H.; Ren, Y. Synthetic strategies for nonporous organosilica nanoparticles from organosilanes. *Nanoscale* **2023**, *15*, 10484–10497. [[CrossRef](#)]
6. Jin, Y.; Li, A.; Hazelton, S.G.; Liang, S.; John, C.L.; Selid, P.D.; Pierce, D.T.; Zhao, J.X. Amorphous silica nanohybrids: Synthesis, properties and applications. *Coord. Chem. Rev.* **2009**, *253*, 2998–3014. [[CrossRef](#)]
7. Qiao, Z.A.; Zhang, L.; Guo, M.; Liu, Y.; Huo, Q. Synthesis of mesoporous silica nanoparticles via controlled hydrolysis and condensation of silicon alkoxide. *Chem. Mater.* **2009**, *21*, 3823–3829. [[CrossRef](#)]
8. Yano, K.; Fukushima, Y. Synthesis of mono-dispersed mesoporous silica spheres with highly ordered hexagonal regularity using conventional alkyltrimethylammonium halide as a surfactant. *J. Mater. Chem.* **2004**, *14*, 1579–1584. [[CrossRef](#)]
9. Yamada, H.; Urata, C.; Ujiie, H.; Yamauchi, Y.; Kuroda, K. Preparation of aqueous colloidal mesostructured and mesoporous silica nanoparticles with controlled particle size in a very wide range from 20 nm to 700 nm. *Nanoscale* **2013**, *5*, 6145–6153. [[CrossRef](#)]
10. Croissant, J.G.; Fatieiev, Y.; Khashab, N.M. Degradability and clearance of silicon, organosilica, silsesquioxane, silica mixed oxide, and mesoporous silica nanoparticles. *Adv. Mater.* **2017**, *29*, 1604634. [[CrossRef](#)]
11. Lin, H.P.; Tsai, C.P. Synthesis of mesoporous silica nanoparticles from a low-concentration CnTMAX-sodium silicate components. *Chem. Lett.* **2003**, *32*, 1092–1093. [[CrossRef](#)]
12. Wan, Y.; Zhao, D. On the controllable soft-templating approach to mesoporous silicates. *Chem. Rev.* **2007**, *107*, 2821–2860. [[CrossRef](#)] [[PubMed](#)]
13. Lelong, G.; Bhattacharyya, S.; Kline, S.; Cacciaguerra, T.; Gonzalez, M.A.; Saboungi, M.L. Effect of surfactant concentration on the morphology and texture of MCM-41 materials. *J. Phys. Chem. C* **2008**, *112*, 10674–10680. [[CrossRef](#)]
14. Chen, B.; Wang, Z.; Quan, G.; Peng, X.; Pan, X.; Wang, R.; Xu, Y.; Li, G.; Wu, C. In vitro and in vivo evaluation of ordered mesoporous silica as a novel adsorbent in liquid formulation. *Int. J. Nanomed.* **2012**, *7*, 199–209.
15. Möller, K.; Bein, T. Talented mesoporous silica nanoparticles. *Chem. Mater.* **2017**, *29*, 371–388. [[CrossRef](#)]
16. Li, X.; Li, X.; Shi, B.; Chaikittisilp, W.; Li, M.; Wang, Y.; Liu, Y.; Gao, L.; Mao, L. A general method to synthesize a family of mesoporous silica nanoparticles less than 100 nm and their applications in anti-reflective/fogging coating. *J. Mater. Sci.* **2016**, *51*, 6192–6206. [[CrossRef](#)]
17. Cai, Q.; Luo, Z.S.; Pang, W.Q.; Fan, Y.W.; Chen, X.H.; Cui, F.Z. Dilute solution routes to various controllable morphologies of MCM-41 silica with a basic medium. *Chem. Mater.* **2001**, *13*, 258–263. [[CrossRef](#)]
18. Lai, C.Y.; Trewyn, B.G.; Jeftinija, D.M.; Jeftinija, K.; Xu, S.; Jeftinija, S.; Lin, V.S.Y. A Mesoporous silica nanosphere-based carrier system with chemically removable CdS nanoparticle caps for stimuli-responsive controlled release of neurotransmitters and drug molecules. *J. Am. Chem. Soc.* **2003**, *125*, 4451–4459. [[CrossRef](#)]
19. Liu, J.; Li, C.; Li, F. Fluorescence turn-on chemodosimeter-functionalized mesoporous silica nanoparticles and their application in cell imaging. *J. Mater. Chem.* **2011**, *21*, 7175–7181. [[CrossRef](#)]
20. Lu, F.; Wu, S.H.; Hung, Y.; Mou, C.Y. Size effect on cell uptake in well-suspended, uniform mesoporous silica nanoparticles. *Small* **2009**, *5*, 1408–1413. [[CrossRef](#)]

21. Lin, Y.S.; Tsai, C.P.; Huang, H.Y.; Kuo, C.T.; Hung, Y.; Huang, D.M.; Chen, Y.C.; Mou, C.Y. Well-ordered mesoporous silica nanoparticles as cell markers. *Chem. Mater.* **2005**, *17*, 4570–4573. [[CrossRef](#)]
22. Yokoi, T.; Karouji, T.; Ohta, S.; Kondo, J.N.; Tatsumi, T. Synthesis of mesoporous silica nanospheres promoted by basic amino acids and their catalytic application. *Chem. Mater.* **2010**, *22*, 3900–3908. [[CrossRef](#)]
23. Zhang, K.; Xu, L.L.; Jiang, J.G.; Calin, N.; Lam, K.F.; Zhang, S.J.; Wu, H.H.; Wu, G.D.; Albela, B.; Bonneviot, L.; et al. Facile large-scale synthesis of monodisperse mesoporous silica nanospheres with tunable pore structure. *J. Am. Chem. Soc.* **2013**, *135*, 2427–2430. [[CrossRef](#)]
24. Lin, H.P.; Mou, C.Y. Structural and morphological control of cationic surfactant-templated mesoporous silica. *Acc. Chem. Res.* **2002**, *35*, 927–935. [[CrossRef](#)]
25. Xiang, W.D.; Yang, Y.X.; Zheng, J.L.; Cao, L.; Ding, H.J.; Liu, X.N. Synthesis of mesoporous silica by cationic surfactant templating in various inorganic acid sources. *Mater. Sci. Pol.* **2010**, *28*, 709–730.
26. Bagshaw, S.A. The effect of dilute electrolytes on the formation of non-ionically templated [Si]-MSU-X mesoporous silica molecular sieves. *J. Mater. Chem.* **2001**, *11*, 831–840. [[CrossRef](#)]
27. Lin, H.P.; Kao, C.P.; Mou, C.Y.; Liu, S.B. Counterion effect in acid synthesis of mesoporous silica materials. *J. Phys. Chem. B* **2000**, *104*, 7885–7894. [[CrossRef](#)]
28. Li, Y.; Wang, Y.; Huang, G.; Ma, X.; Gao, I. A surprising chaotropic anion-induced supramolecular self-assembly of ionic polymeric micelles. *Angew. Chem. Int. Ed.* **2014**, *53*, 8074–8078. [[CrossRef](#)] [[PubMed](#)]
29. Yu, C.; Fan, J.; Tian, B.; Zhao, D.; Stucky, G.D. High-yield synthesis of periodic mesoporous material. *Adv. Mater.* **2002**, *14*, 1742–1745. [[CrossRef](#)]
30. Issa, A.A.; Luyt, A.S. Kinetics of alkoxysilanes and organoalkoxysilanes polymerization: A review. *Polymers* **2019**, *11*, 537. [[CrossRef](#)] [[PubMed](#)]
31. Yu, C.; Tian, B.; Fan, J.; Stucky, G.D.; Zhao, D. Salt effect in the synthesis of mesoporous silica templated by non-ionic block copolymers. *Chem. Commun.* **2001**, *24*, 2726–2727. [[CrossRef](#)]
32. Yu, C.; Fan, J.; Tian, B.; Zhao, D. Morphology development of mesoporous materials: A colloidal phase separation mechanism. *Chem. Mater.* **2004**, *16*, 889–898. [[CrossRef](#)]
33. Trompette, J.L. Influence of co-ion nature on the gelation kinetics of colloidal silica suspensions. *J. Phys. Chem. B* **2017**, *121*, 5654–5659. [[CrossRef](#)] [[PubMed](#)]
34. Van Der Linden, M.; Conchúir, B.O.; Spigone, E.; Niranjana, A.; Zaccone, A.; Cicuta, P. Microscopic origin of the Hofmeister effect in gelation kinetics of colloidal silica. *J. Phys. Chem. Lett.* **2015**, *6*, 2881–2887. [[CrossRef](#)]
35. Tadros, T.F.; Lyklema, J. Adsorption of potential-determining ions at the silica-aqueous electrolyte interface and the role of some cations. *J. Electroanal. Chem. Interfacial Electrochem.* **1968**, *17*, 267–275. [[CrossRef](#)]
36. Matsoukas, T.; Gulari, E. Dynamics of growth of silica particles from ammonia-catalyzed hydrolysis of tetra-ethyl-orthosilicate. *J. Colloid Interface Sci.* **1988**, *124*, 252–261. [[CrossRef](#)]
37. Zainal, N.A.; Shukor, S.R.A.; Wab, H.A.A.; Razak, K.A. Study on the effect of synthesis parameters of silica nanoparticles entrapped with rifampicin. *Chem. Eng. Trans.* **2013**, *32*, 2245–2250.
38. Issa, A.A.; El-Azazy, M.; Luyt, A.S. Kinetics of alkoxysilanes hydrolysis: An empirical approach. *Sci. Rep.* **2019**, *9*, 17624. [[CrossRef](#)] [[PubMed](#)]
39. Yamada, Y.; Yano, K. Synthesis of monodispersed super-microporous/mesoporous silica spheres with diameters in the low submicron range. *Micropor. Mesopor. Mater.* **2006**, *93*, 190–198. [[CrossRef](#)]
40. Gu, J.; Huang, K.; Zhu, X.; Li, Y.; Wei, J.; Zhao, W.; Liu, C.; Shi, J. Sub-150 nm mesoporous silica nanoparticles with tunable pore sizes and well-ordered mesostructure for protein encapsulation. *J. Colloid Interface Sci.* **2013**, *407*, 236–242. [[CrossRef](#)]
41. Yang, B.; Chen, Y.; Shi, J. Mesoporous silica/organosilica nanoparticles: Synthesis, biological effect and biomedical application. *Mater. Sci. Eng. R* **2019**, *137*, 66–105. [[CrossRef](#)]
42. Lee, C.H.; Park, S.H.; Chung, W.; Kim, J.Y.; Kim, S.H. Preparation and characterization of surface-modified silica nanoparticles with organo-silane compounds. *Colloids Surf. A* **2011**, *384*, 318–322. [[CrossRef](#)]
43. Kim, K.M.; Kim, H.M.; Lee, W.J.; Lee, C.W.; Kim, T.-I.; Lee, J.K.; Jeong, J.; Paek, S.M.; Oh, J.M. Surface treatment of silica nanoparticles for stable and charge-controlled colloidal silica. *Int. J. Nanomed.* **2014**, *9*, 29–40.
44. Croissant, J.G.; Cattoën, X.; Durand, J.O.; Wong Chi Man, M.; Khashab, N.M. Organosilica hybrid nanomaterials with a high organic content: Syntheses and applications of silsesquioxanes. *Nanoscale* **2016**, *8*, 19945–19972. [[CrossRef](#)] [[PubMed](#)]
45. Arkhireeva, A.; Hay, J.N. Synthesis of sub-200 nm silsesquioxane particles using a modified Stöber sol–gel route. *J. Mater. Chem.* **2003**, *13*, 3122–3127. [[CrossRef](#)]
46. Dirè, S.; Tagliuzucca, V.; Callone, E.; Quaranta, A. Effect of functional groups on condensation and properties of sol–gel silica nanoparticles prepared by direct synthesis from organoalkoxysilanes. *Mater. Chem. Phys.* **2011**, *126*, 909–917. [[CrossRef](#)]
47. Arkhireeva, A.; Hay, J.N.; Lane, J.M.; Manzano, M.; Masters, H.; Oware, W.; Shaw, S.J. Synthesis of organic-inorganic hybrid particles by sol-gel chemistry. *J. Sol-Gel Sci. Technol.* **2004**, *31*, 31–36. [[CrossRef](#)]
48. Takahashi, K.; Tadanaga, K.; Hayashi, A.; Tatsumisago, M. Preparation and characterization of polyaminophenylsilsesquioxane particles by two-step acid–base-catalyzed sol–gel process. *Chem. Lett.* **2007**, *2*, 324–325. [[CrossRef](#)]
49. Wang, L.; Tan, W. Multicolor FRET silica nanoparticles by single wavelength excitation. *Nano Lett.* **2006**, *6*, 84–88. [[CrossRef](#)]

50. Zhang, W.H.; Hu, X.X.; Zhang, X.B. Dye-doped fluorescent silica nanoparticles for live cell and in vivo bioimaging. *Nanomater.* **2016**, *6*, 81. [[CrossRef](#)]
51. Wang, C.; Yan, J.; Cui, X.; Wang, H. Synthesis of raspberry-like monodisperse magnetic hollow hybrid nanospheres by coating polystyrene template with Fe<sub>3</sub>O<sub>4</sub>@SiO<sub>2</sub> particles. *J. Colloid Interface Sci.* **2011**, *354*, 94–99. [[CrossRef](#)] [[PubMed](#)]
52. Zheng, J.; Liu, Q.; Wei, W.; Lu, Y.; Wang, S.; Chen, H.; Zhou, Y. Roughness surface of raspberry-shaped silica nanoparticles effect on shear thickening colloidal suspensions. *Appl. Surf. Sci.* **2022**, *606*, 154917. [[CrossRef](#)]
53. Du, X.; He, J. A self-templated etching route to surface-rough silica nanoparticles for superhydrophobic coatings. *ACS Appl. Mater. Interfaces* **2011**, *3*, 1269–1276. [[CrossRef](#)] [[PubMed](#)]
54. Li, X.; He, J. In situ assembly of raspberry-and mulberry-like silica nanospheres toward antireflective and antifogging coatings. *ACS Appl. Mater. Interfaces* **2012**, *4*, 2204–2211. [[CrossRef](#)]
55. Zhao, Z.B.; Zhang, D.M.; Meng, Y.F.; Tai, L.; Jiang, Y. One-pot fabrication of fluoride-silica@ silica raspberry-like nanoparticles for superhydrophobic coating. *Ceram. Int.* **2016**, *42*, 14601–14608. [[CrossRef](#)]
56. Semeykina, V.S.; Zharov, I. Medium-controlled aggregative growth as a key step in mesoporous silica nanoparticle formation. *J. Colloid Interface Sci.* **2022**, *615*, 236–247. [[CrossRef](#)]
57. Vivero-Escoto, J.L.; Slowing, I.I.; Trewyn, B.G.; Lin, V.S.-Y. Mesoporous silica nanoparticles for intracellular controlled drug delivery. *Small* **2010**, *6*, 1952–1967. [[CrossRef](#)]
58. Manzano, M.; Vallet-Regí, M. Mesoporous silica nanoparticles for drug delivery. *Adv. Funct. Mater.* **2020**, *30*, 1902634. [[CrossRef](#)]
59. Feldmann, V.; Engelmann, J.; Gottschalk, S.; Mayer, H.A. Synthesis, characterization and examination of Gd [DO3A-hexylamine]-functionalized silica nanoparticles as contrast agent for MRI-applications. *J. Colloid Interface Sci.* **2012**, *366*, 70–79. [[CrossRef](#)]
60. Cha, B.G.; Kim, J. Functional mesoporous silica nanoparticles for bio-imaging applications. *Wiley Interdiscip. Rev. Nanomed. Nanobiotechnol.* **2019**, *11*, e1515. [[CrossRef](#)]
61. Niculescu, V.C. Mesoporous silica nanoparticles for bio-applications. *Front. Mater.* **2020**, *7*, 36. [[CrossRef](#)]
62. Brozek, E.M.; Zharov, I. Internal functionalization and surface modification of vinylsilsesquioxane nanoparticles. *Chem. Mater.* **2009**, *21*, 1451–1456. [[CrossRef](#)]
63. Tripathi, V.S.; Kandimalla, V.B.; Ju, H. Preparation of Ormosil and its applications in immobilizing biomolecules. *Sens. Actuators B* **2006**, *114*, 1071–1082. [[CrossRef](#)]
64. Gonçalves, M.C. Sol-gel silica nanoparticles in medicine: A natural choice. Design, synthesis and products. *Molecules* **2018**, *23*, 2021. [[CrossRef](#)] [[PubMed](#)]
65. Soloway, A.H.; Tjarks, W.; Barnum, B.A.; Rong, F.-G.; Barth, R.F.; Codogni, I.M.; Wilson, J.G. The chemistry of neutron capture therapy. *Chem. Rev.* **1998**, *98*, 1515–1562. [[CrossRef](#)] [[PubMed](#)]
66. Gao, Z.; Moghaddam, S.P.H.; Ghandehari, H.; Zharov, I. Synthesis of water-degradable silica nanoparticles from carbamate-containing bridged silsesquioxane precursor. *RSC Adv.* **2018**, *8*, 4914–4920. [[CrossRef](#)]
67. Gao, Z.; Zharov, I. Large pore mesoporous silica nanoparticles by templating with a nonsurfactant molecule, tannic acid. *Chem. Mater.* **2014**, *26*, 2030–2037. [[CrossRef](#)]
68. Brozek, E.M.; Washton, N.M.; Mueller, K.T.; Zharov, I. Silsesquioxane particles with internal functional groups. *J. Nanopart. Res.* **2017**, *19*, 85–97. [[CrossRef](#)]
69. Walton, N.I.; Gao, Z.; Zharov, I. Theranostic anticancer agents based on internally functionalized ORMOSIL nanoparticles. *MRS Proc.* **2014**, *1526*, 215–221. [[CrossRef](#)]
70. Walton, N.I.; Naha, P.; Cormode, D.P.; Zharov, I. Mesoporous organosilica nanoparticles with internal metal-chelating groups: Transition metal uptake and Gd<sup>3+</sup> relaxivity. *Chem. Sel.* **2023**, *8*, e202301454. [[CrossRef](#)]
71. Ottenbrite, R.M.; Wall, J.S.; Siddiqui, J.A. Self-catalyzed synthesis of organo-silica nanoparticles. *J. Am. Ceram. Soc.* **2000**, *83*, 3214–3215. [[CrossRef](#)]
72. Stöber, W.; Fink, A.; Bohn, E.J. Controlled growth of monodisperse silica spheres in the micron size range. *J. Colloid Interface Sci.* **1968**, *26*, 62–69. [[CrossRef](#)]
73. Gu, J.; Fan, W.; Shimojima, A.; Okubo, T. Organic–inorganic mesoporous nanocarriers integrated with biogenic ligands. *Small* **2007**, *3*, 1740–1744. [[CrossRef](#)]
74. Wang, Y.; Zhang, B.; Ding, X.; Du, X. Dendritic mesoporous organosilica nanoparticles (DMONs): Chemical composition, structural architecture, and promising applications. *Nano Today* **2021**, *39*, 101231. [[CrossRef](#)]
75. Hartono, S.B.; Gu, W.; Kleitz, F.; Liu, J.; He, L.; Middelberg, A.P.J.; Yu, C.; Lu, G.Q.; Qiao, S.Z. Poly-L-lysine functionalized large pore cubic mesostructured silica nanoparticles as biocompatible carriers for gene delivery. *ACS Nano* **2012**, *6*, 2104–2117. [[CrossRef](#)]
76. Barrett, E.P.; Joyner, L.G.; Halenda, P.P. The determination of pore volume and area distributions in porous substances. I. Computations from nitrogen isotherms. *J. Am. Chem. Soc.* **1951**, *73*, 373–380. [[CrossRef](#)]
77. Xu, C.; Lei, C.; Wang, Y.; Yu, C. Dendritic mesoporous nanoparticles: Structure, synthesis and properties. *Angew. Chem. Int. Ed.* **2022**, *61*, e202112752. [[CrossRef](#)] [[PubMed](#)]
78. Sing, K.S. Reporting physisorption data for gas/solid systems with special reference to the determination of surface area and porosity. *Pure Appl. Chem.* **1985**, *57*, 603–619. [[CrossRef](#)]
79. Xie, J.; Lee, S.; Chen, X. Nanoparticle-based theranostic agents. *Adv. Drug Deliv. Rev.* **2010**, *62*, 1064–1079. [[CrossRef](#)]

80. Fernandes, N.B.; Nayak, Y.; Garg, S.; Nayak, U.Y. Multifunctional engineered mesoporous silica/inorganic material hybrid nanoparticles: Theranostic perspectives. *Coord. Chem. Rev.* **2023**, *478*, 214977. [[CrossRef](#)]
81. Pontón, I.; del Rio, A.M.; Gómez, M.G.; Sánchez-García, D. Preparation and applications of organo-silica hybrid mesoporous silica nanoparticles for the co-delivery of drugs and nucleic acids. *Nanomaterials* **2020**, *10*, 2466. [[CrossRef](#)] [[PubMed](#)]
82. Huang, P.; Qian, X.; Chen, Y.; Yu, L.; Lin, H.; Wang, L.; Zhu, Y.; Shi, J. Metalloporphyrin-encapsulated biodegradable nanosystems for highly efficient magnetic resonance imaging-guided sonodynamic cancer therapy. *J. Am. Chem. Soc.* **2017**, *139*, 1275–1284. [[CrossRef](#)] [[PubMed](#)]
83. Freitas, V.T.; Fu, L.; Cojocariu, A.M.; Cattoën, X.; Bartlett, J.R.; Le Parc, R.; Bantignies, J.L.; Wong Chi Man, M.; André, P.S.; Ferreira, R.A.S.; et al. Eu<sup>3+</sup>-based bridged silsesquioxanes for transparent luminescent solar concentrators. *ACS Appl. Mater. Interfaces* **2015**, *7*, 8770–8778. [[CrossRef](#)] [[PubMed](#)]
84. Correia, S.F.H.; Lima, P.P.; André, P.S.; Ferreira, M.R.S.; Carlos, L.A.D. High-efficiency luminescent solar concentrators for flexible waveguiding photovoltaics. *Sol. Energy Mater. Sol. Cells* **2015**, *138*, 51–57. [[CrossRef](#)]
85. Ferré, M.; Pleixats, R.; Wong Chi Man, M.; Cattoën, X. Recyclable organocatalysts based on hybrid silicas. *Green Chem.* **2016**, *18*, 881–922. [[CrossRef](#)]
86. Zhao, L.; Zhang, Y.; Yang, Y.; Yu, C. Silica-based nanoparticles for enzyme immobilization and delivery. *Chem. Asian J.* **2022**, *17*, e202200573. [[CrossRef](#)]
87. Nuruzzaman, M.; Ren, J.; Liu, Y.; Rahman, M.M.; Shon, H.K.; Naidu, R. Hollow porous silica nanosphere with single large pore opening for pesticide loading and delivery. *ACS Appl. Nano Mater.* **2020**, *3*, 105–113. [[CrossRef](#)]
88. Chen, X.; Liu, J.; Ma, Y.; Wang, P.; Bai, X.; Pan, J. Large-scale and low-cost fabrication of two functional silica sorbents by vapor condensation induced nanoemulsions and their excellent uptake performance. *Chem. Eng. J.* **2020**, *379*, 122364. [[CrossRef](#)]

**Disclaimer/Publisher's Note:** The statements, opinions and data contained in all publications are solely those of the individual author(s) and contributor(s) and not of MDPI and/or the editor(s). MDPI and/or the editor(s) disclaim responsibility for any injury to people or property resulting from any ideas, methods, instructions or products referred to in the content.